Supplementary Information for "Superconductivity in an electron band just above the Fermi level: possible route to BCS-BEC superconductivity"

K. Okazaki[1],[*] Y. Ito[1], Y. Ota[1], Y. Kotani[1],[†] T. Shimojima[1],[‡] T. Kiss[1],[§] S. Watanabe[2], C. -T. Chen[3], S. Niitaka[4,5], T. Hanaguri[4,5], H. Takagi[4,5], A. Chainani[6,7], and S. Shin[1,5,6,8]

[1]*Institute for Solid State Physics (ISSP), University of Tokyo, Kashiwa, Chiba 277-8581, Japan*

[2]*Research Institute for Science and Technology, Tokyo University of Science, Chiba 278-8510, Japan*

[3]*Beijing Center for Crystal R&D, Chinese Academy of Science (CAS), Zhongguancun, Beijing 100190, China*

[4]*RIKEN Advanced Science Institute, 2-1, Hirosawa, Wako, Saitama 351-0198, Japan*

[5]*TRIP, JST, Chiyoda-ku, Tokyo 102-0075, Japan*

[6]*RIKEN SPring-8 Center, Sayo-gun, Hyogo 679-5148, Japan*

[7]*Department of Physics, Tohoku University, Aramaki, Aoba-ku, Sendai 980-8578 Japan*

[8]*CREST, JST, Chiyoda-ku, Tokyo 102-0075, Japan*

Band-structure calculations and dominant orbital characters

Figure S1(a) shows band dispersions calculated by the Wien2k code for the pure FeTe. The lattice parameters were taken from those obtained by the powder neutron diffraction measurements [38] as in the previous report by Miyake *et al.* [39]. We confirmed that the obtained band dispersions are in accord with those by Miyake *et al.* We deduced the dominant orbital contribution of each band as indicated by different colors. Figure S1(b) shows the enlarged band dispersions in the vicinity of E_F along the measured X-Γ-X line. The 28th, 29th, and 30th bands show hole-like dispersions and cross the E_F, whereas the 31st band shows a electron-like dispersion just above E_F around the Γ point.

Orbital characters from polarization dependent measurements

Figure S2(a) shows the experimental configuration of the laser ARPES measurements for this study. In this configuration, xy and yz orbitals can be measured only for the p polarization, whereas the $x^2 - y^2$, z^2, and xz orbitals can be measured for both the polarizations from the parity selection rule [40]. By taking account of the parity of each d orbital and orbital characters obtained from the band-structure calculation, we assigned the dominant orbital characters of the observed three hole bands as well as the electron band just above E_F, as shown in Fig. S2(c).

Determination of the band dispersions above E_F from three different methods

We used three different methods to determine the band dispersions above E_F at 25 K as described in the following. Each method has its own advantages and disadvantages. However, the three methods provide consistent band dispersions, and we can safely conclude that an electron band exists just above E_F at the Γ point. We could then determine the positions of the bottom of the electron band and the top of $x^2 - y^2$ hole band.

Second derivative spectra with respect to energy

Figure S3(a) shows a second derivative map with respect to energy obtained from the map shown in Fig. 1(a). The open circles indicate the peak positions. Figure S3(b) is

obtained by first dividing the intensity map by the Fermi-Dirac (FD) function at $T = 25$ K broadened with the experimental energy resolution, and then taking the second derivative.

Fitting to EDCs

Figure S4 shows the results of fitting to several EDC cuts along the X-Γ-X direction without dividing by the FD function. The solid lines indicate the fitting results. The fitting functions were obtained by first multiplying the FD function to the three Lorentzians, and then taking the convolution with the Gaussian corresponding to the experimental energy resolution.

Fitting to MDCs

Figures S5(a) and S5(b) show the results of fitting to several cuts of MDCs at (a) 25 K and (b) 2.5 K, respectively, after dividing by the FD function convoluted with the Gaussian. We note that dividing by the FD function does not affect the lineshape of MDCs. The solid lines and vertical bars indicate the fitting functions and their peak positions. The fitting was performed in the region of $k \geq 0$ with the symmetrized Lorentzians to avoid matrix element effects, i.e., the MDC fitting function $I(\omega)$ is given by $I(\omega) = \sum_i I_i(k) + \sum_i I_i(-k)$, where $I_i(k)$ is a component Lorentzian.

Band dispersions determined by various methods

Figures S6(a) and S6(b) show the E-k map measured at (a) 25 K and (b) 2.5 K, respectively. The open circles, rectangles, and triangles indicate the band dispersions determined by the second derivative spectra, fitting to the EDCs, and fitting to the MDCs. As mentioned above, each of these methods has advantages and disadvantages. Because the peak positions of the second derivative spectra are located where the gradient of the spectra shows large changes, it can detect the lower-energy side of the dispersion around the Γ point. The fitting to the EDCs is the most appropriate to determine the band dispersion where the gradient of the dispersion is small, but it is difficult to determine the dispersions above E_F without ambiguity. On the other hand, there is no ambiguity for the peak positions of

MDCs even for those above E_F, but it is difficult to determine the dispersions around the top and bottom of the bands from MDC fits. However, the combination of three methods allows us to conclude that the top of the hole band is located at 6-7 meV above E_F and an electron band exists just above E_F for the dispersions at 25 K. At 2.5 K, we can recognize the superconducting coherence peaks separately at $k = k_F$ and the Γ point.

Fitting to EDCs at higher temperatures

We performed measurements with another sample at higher temperatures of 35 K and 50 K in addition to 25 K. Figures S7(a)-(c) show the FD-divided EDCs at the Γ point for these temperatures. The solid lines indicate the fitting functions which are the same as those used in Fig. 1(c), and the dashed lines are the component Lorentzians. The peak positions are consistent with data shown in Fig. 1, although the relative intensities of the two peaks are different. Figure S7(d) shows the FD-divided EDCs along the Γ-X line at 50 K and the corresponding intensity plot is shown in Fig. S7(e). The rectangles indicate the band dispersions deduced from the fitting to the EDCs in the same way as Fig. 1(b). The solid lines are the same as those in Fig. 1(b) and extended up to 20 meV above E_F. It confirms that the band dispersions at 50 K are consistent with the band dispersions at 25 K.

Polarization dependent spectra below T_c and above T_c

Figures S8 and S9 show the polarization-dependent intensity map and second derivative map measured below T_c (= 2.5 K) and above T_c (= 25 K), respectively. They were measured with right circular, left circular, s-, and p-polarizations. As described above in the section of **"Orbital characters from polarization dependent measurements"**, the orbitals with the odd parity can be measured with the p-polarization. In the second derivative spectra below T_c, a clear feature at Γ point can be seen only for the p-polarization just below E_F, while the structure for k_F crossings away from Γ point can be seen for the both polarizations. This indicates a difference in orbital characters between the $x^2 - y^2$ hole band and the electron band just above E_F. The right and left circular polarizations were used to avoid the selection rules for bands of particular symmetry which arise in photoemission with linear polarization. This ensures we have measured all the band dispersions with minimal

matrix element effects.

Dispersion of the superconducting coherence peak around the Γ point

The superconducting coherence peaks and BQP dispersions shown in Figs. 2(b) and 2(g) were enlarged in Fig. S10. These plots clearly shows that the coherence peaks at $k \sim \Gamma$ is originated from the electron band just above E_F. The BQP disperion originated from the $x^2 - y^2$ hole band is almost flat around $k = \pm 0.1$ Å^{-1} and shows an indication of a bending-back behaviour, while the curvature of the dispersion around $k \sim \Gamma$ is very different from the almost flat dispersion of the BQP originated from the $x^2 - y^2$ hole band and corresponds a reflection of the electronic dispersion just above E_F in the normal state.

Temperature dependence of symmetrized EDCs and FD-divided EDCs

The temperature dependent EDCs shown in Fig. 3 were symmetrized with respect to E_F and the results are shown in Fig. S11, and they were divided by the FD functions of corresponding temperatures and the results are shown in Fig. S12. The existence of the pseudogap for the $x^2 - y^2$ hole band can be clearly recognized also from both symmetrized EDCs and FD-divided EDCs as well as the temperature dependence of the SC-gap size estimated from fitting.

* Present address: Department of Physics, University of Tokyo, Tokyo 113-0033, Japan; Electronic address: okazaki@wyvern.phys.s.u-tokyo.ac.jp

† Present address: Japan Synchrotron Radiation Research Institute (JASRI/SPring-8), Sayo, Hyogo 679-5198, Japan

‡ Present address: Department of Applied Physics, University of Tokyo, Tokyo 113-8656, Japan

§ Present address: Graduate School of Engineering Science, Osaka University, Osaka 560-8531, Japan

[38] Li, S. et al. First-order magnetic and structural phase transitions in $Fe_{1+y}Se_xTe_{1-x}$. *Phys. Rev. B* **79**, 054503 (2009).

[39] Miyake, T., Nakamura, K., Arita, R., and Imada, M. Comparison of *Ab initio* Low-Energy Models for LaFePO, LaFeAsO, $BaFe_2As_2$, LiFeAs, FeSe, and FeTe: Electron Correlation and Covalency. *J. Phys. Soc. Jpn* **79**, 044705 (2010).

[40] Damascelli, A., Hussain, Z., and Shen, Z.-X. Angle-resolved photoemission studies of the cuprate superconductors. *Rev. Mod. Phys.* **75**, 473–541 (2003).

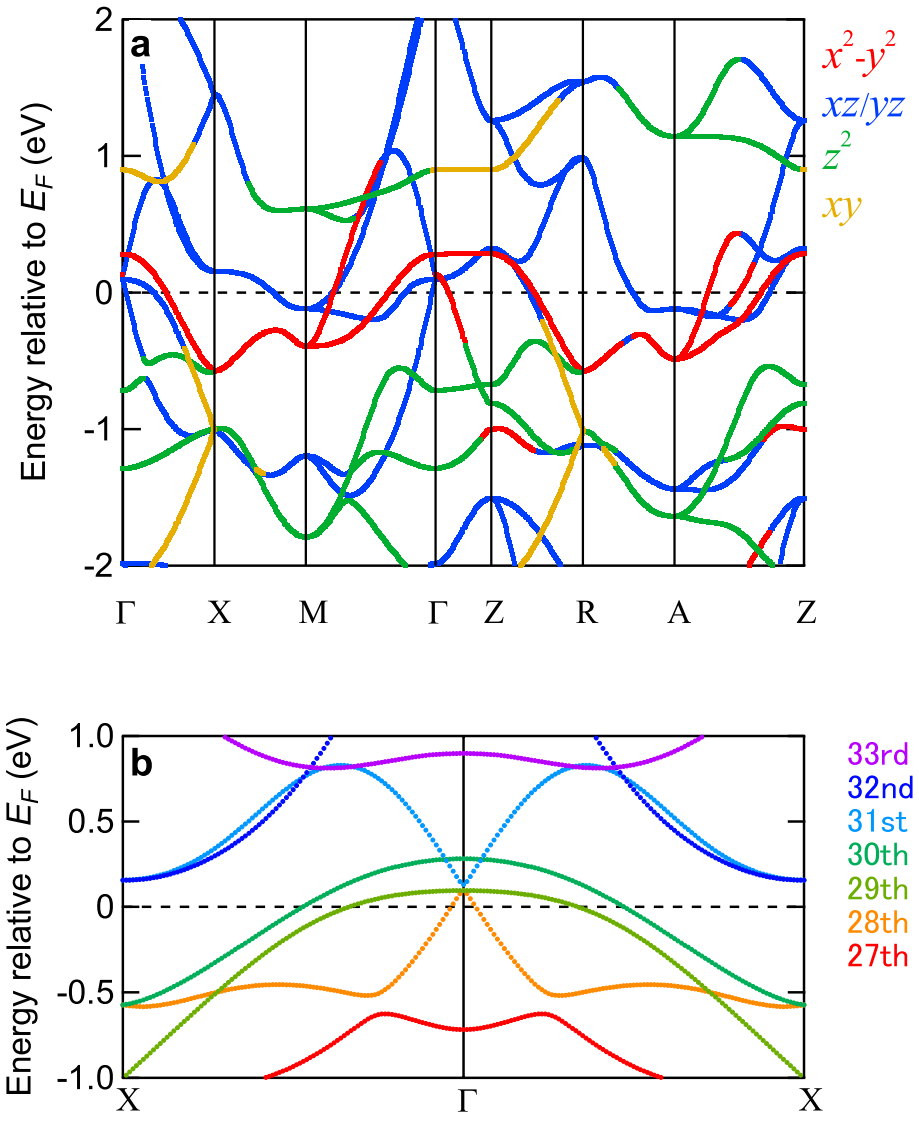

Fig. S1. Band-structure calculations for the parent FeTe based on the density functional theory. (**a**), Band dispersion along the high symmetric line in the Brillouin zone calculated by Wien2k code. The dominant orbital character of each band is indicated by different colors. The bands near the E_F are mainly composed of $x^2 - y^2$ and xz/yz orbitals. (**b**), Band dispersion near the E_F is along the X-Γ-X line. The 28th, 29th, and 30th bands show hole-like dispersions and cross the E_F, whereas the 31st band shows a electron-like dispersion just above E_F around the Γ point. The dispersion of the 28th and 31st bands looks like a Dirac cone.

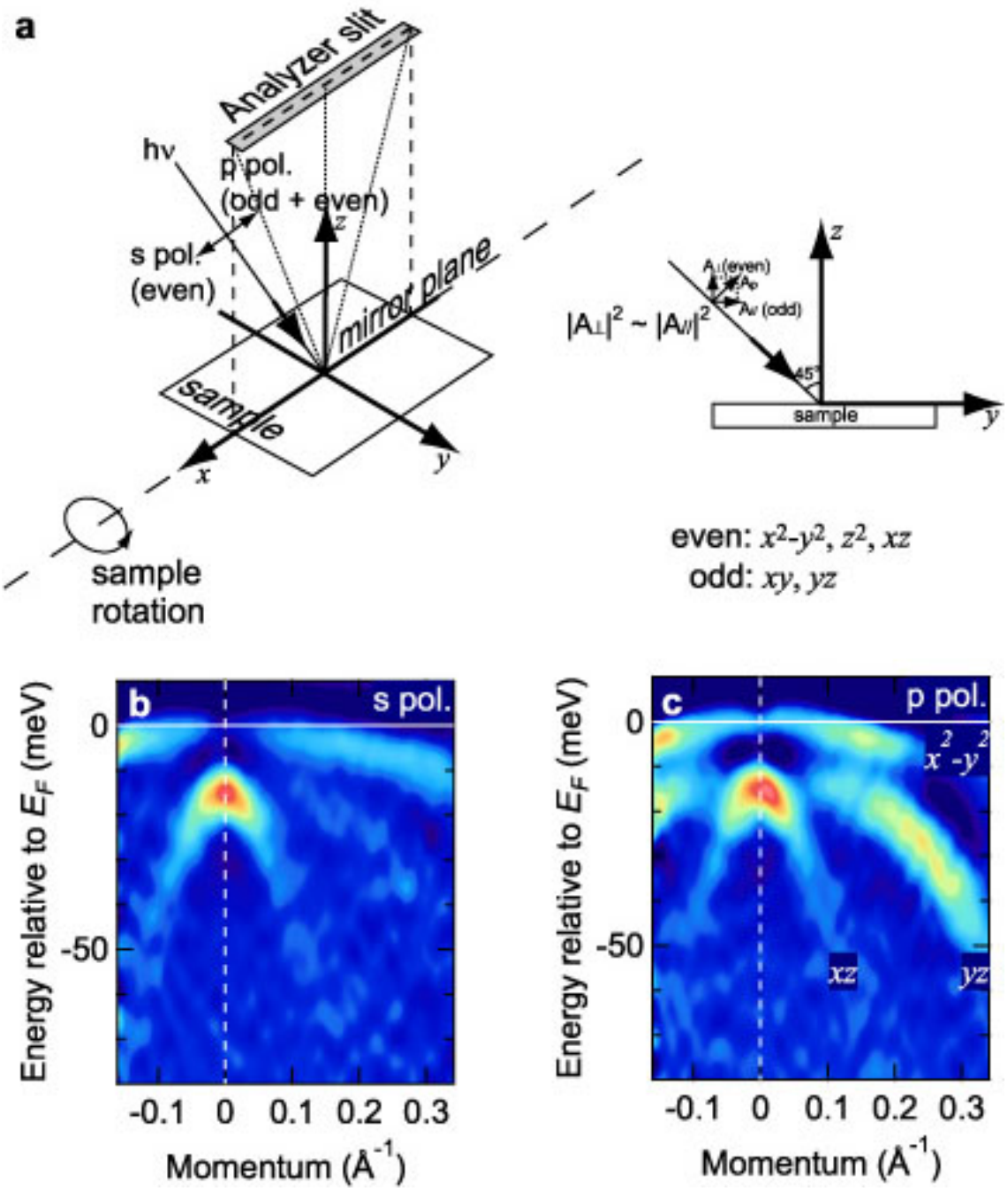

Fig. S2. Experimental configuration and linear-polarization dependence of ARPES intensity. (**a**), Experimental configuration and parity of each d orbital with respect to the mirror plane including the analyzer slit. ARPES intensity plotted as a function of momentum and energy measured at 25 K with (**b**) s- and (**c**) p-polarizations, respectively. Dominant d orbital for each band is indicated in (c).

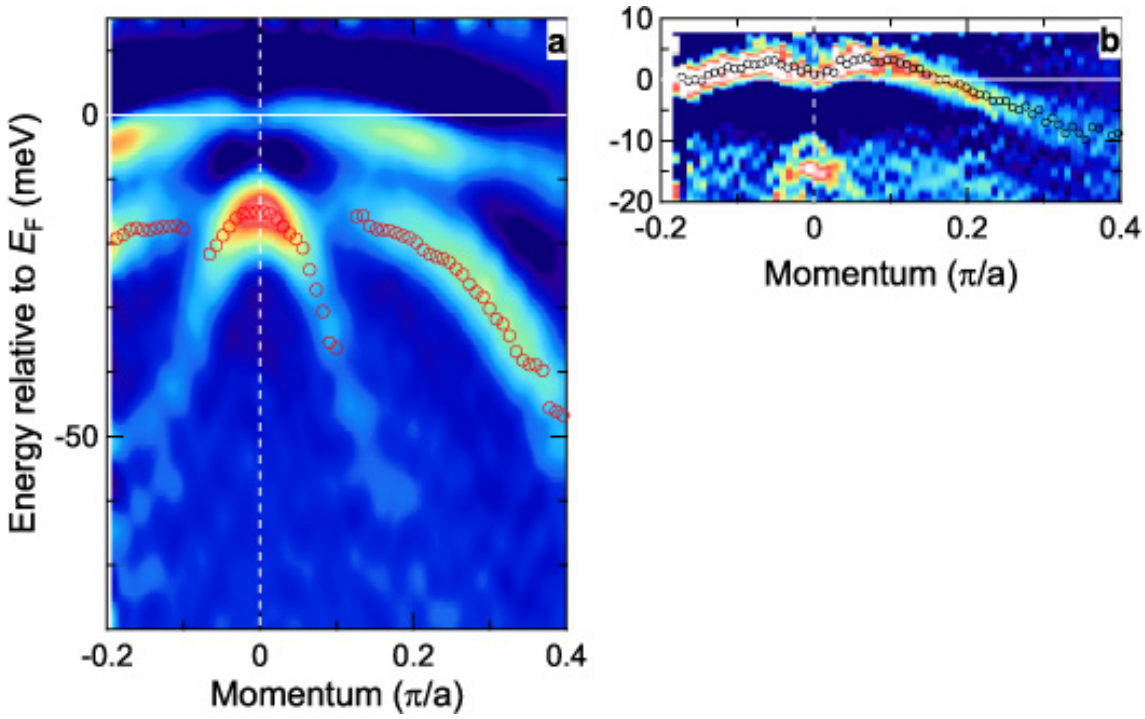

Fig. S3. Band dispersions from the second derivative spectra (**a**), Second derivative map with respect to energy. (**b**), Second derivative map after dividing by the FD function convoluted with a Gaussian of the experimental resolution. The open circles indicate band dispersions deduced from the peak positions of each map.

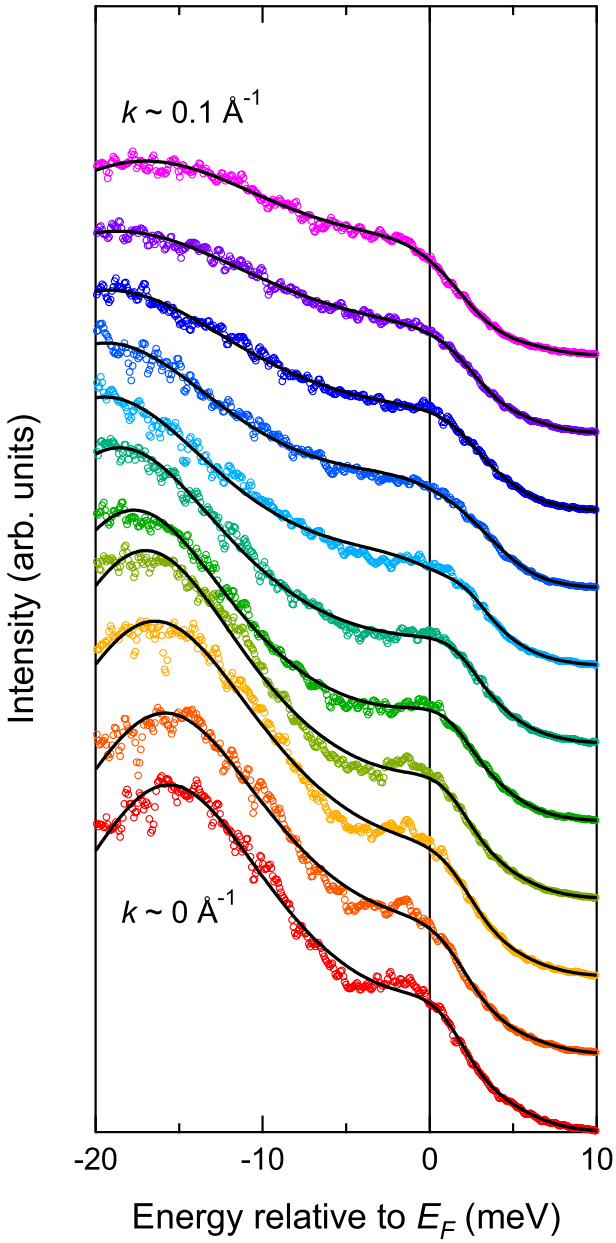

Fig. S4. Fitting to several cuts of EDCs along the Γ-X line without dividing by the FD function. The solid lines indicate the fitting results.

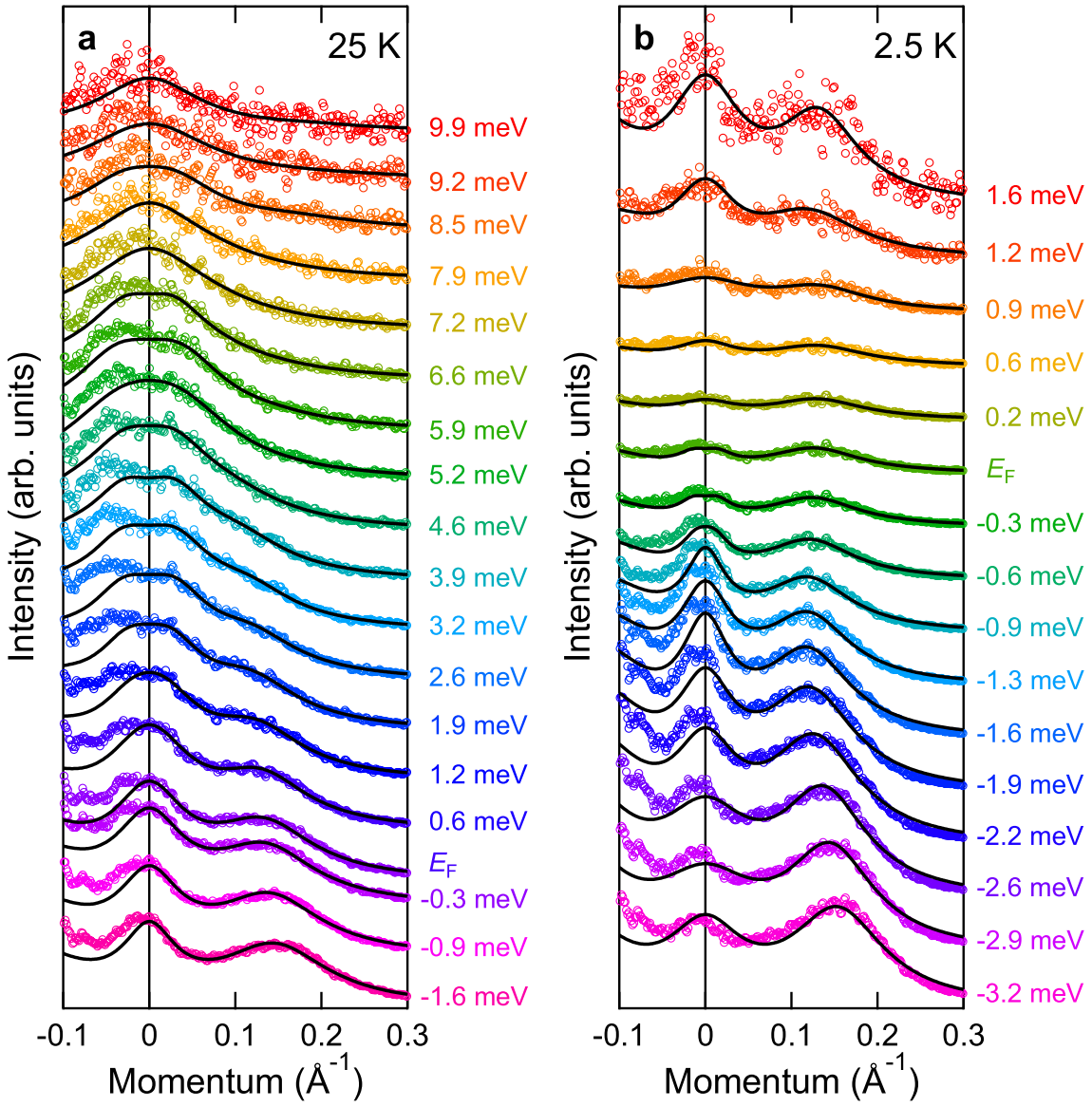

Fig. S5. Fits to several cuts of MDCs along the Γ-X line. **a** MDCs at 25 K. **b** MDCs at 2.5 K.

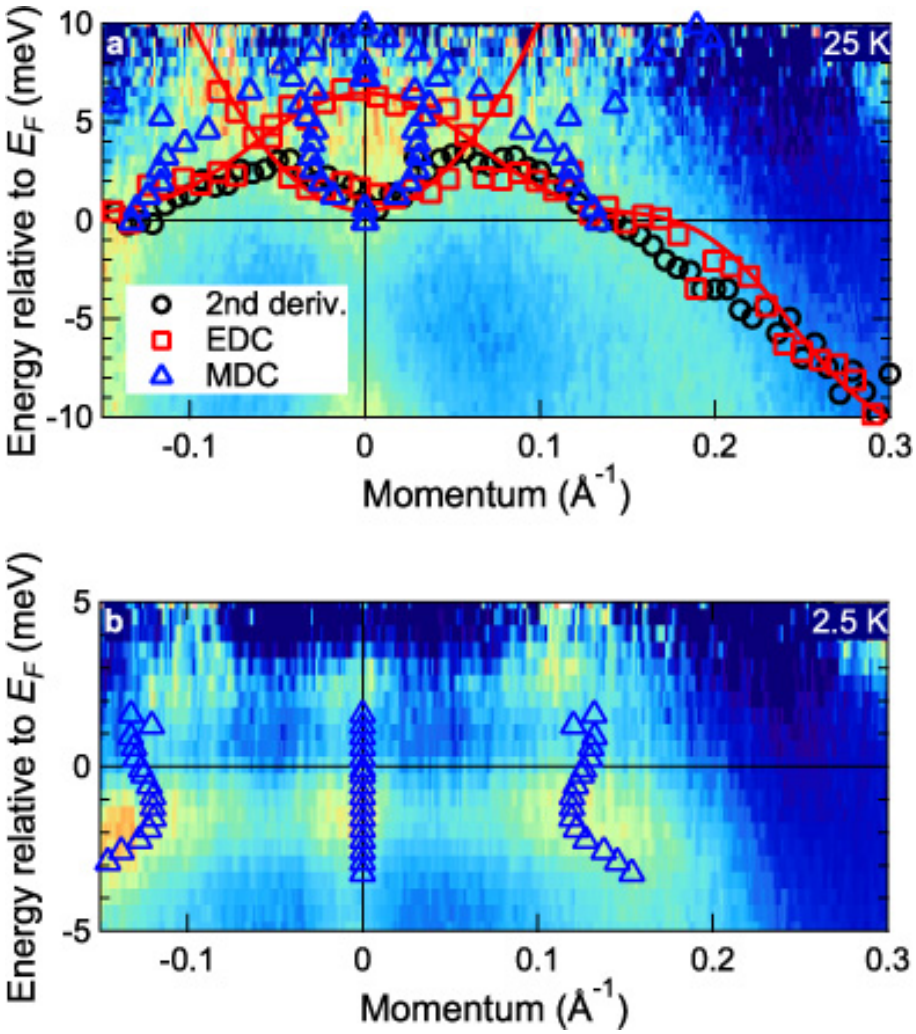

Fig. S6. Band dispersions determined by three methods. (**a** and **b**), E-k map measured at (a) 25 K and (b) 2.5K. Black circles, red rectangles, blue triangles are determined by the second derivative spectra, fitting to the EDCs, and fitting to the MDCs, respectively.

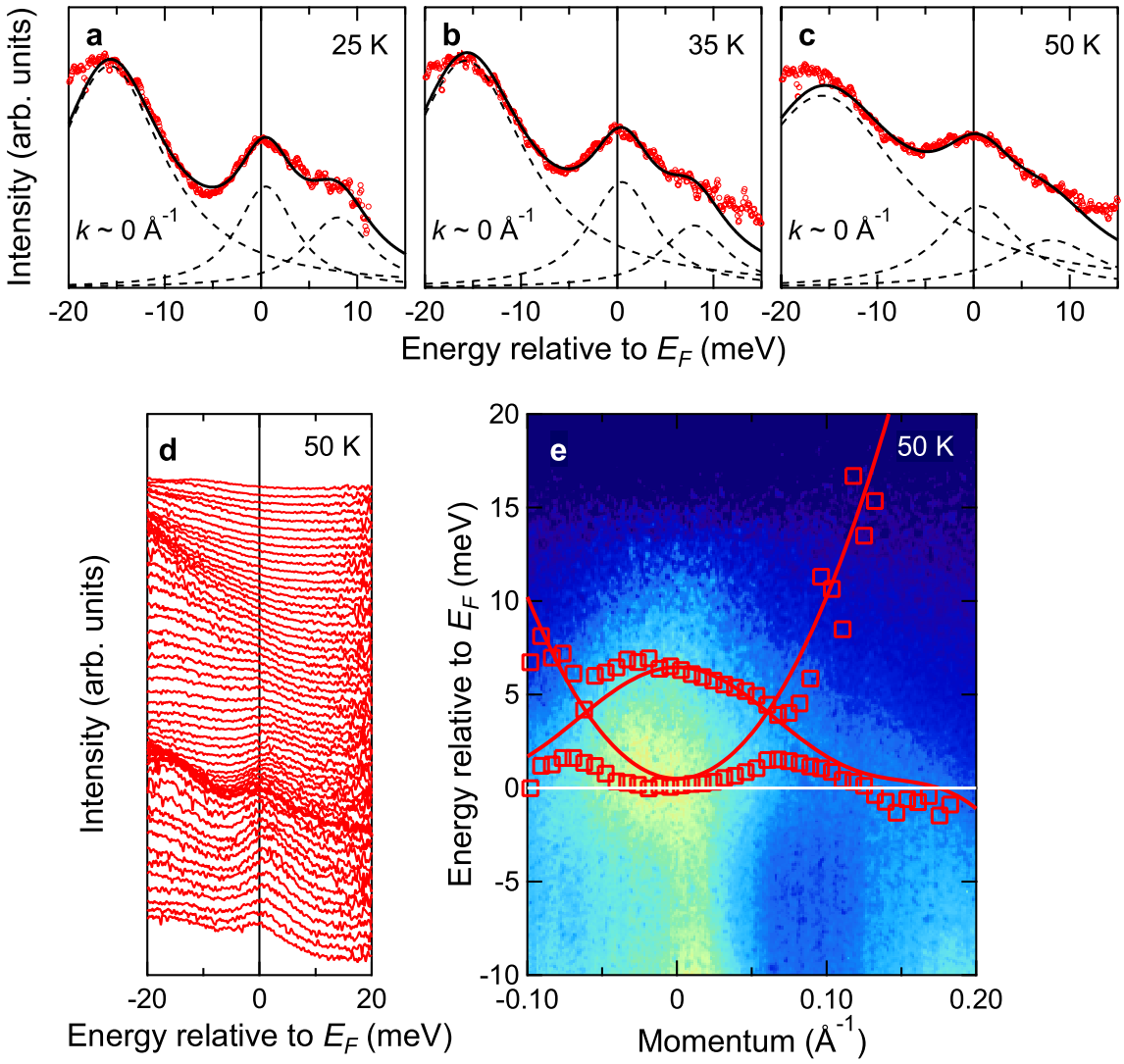

Fig. S7. Fitting to FD-divided EDCs at higher temperatures. (**a**-**c**), FD-divided EDCs at the Γ point measured at 25 K (a), 35 K (b), and 50 K (c) for another sample. The solid and dashed lines indicate the fitting functions and component Lorentzians. (**d**) FD-divided EDCs along the Γ-X line at 50 K. (**e**) Intensity plot of the ARPES spectra at 50 K. The rectangles indicate the band dispersions deduced from the fitting to the EDCs in the same way as Fig. 1(b). The solid lines are the same as those in Fig. 1(b), thereby confirming that the band dispersions at 50 K are consistent with the band dispersions at 25 K.

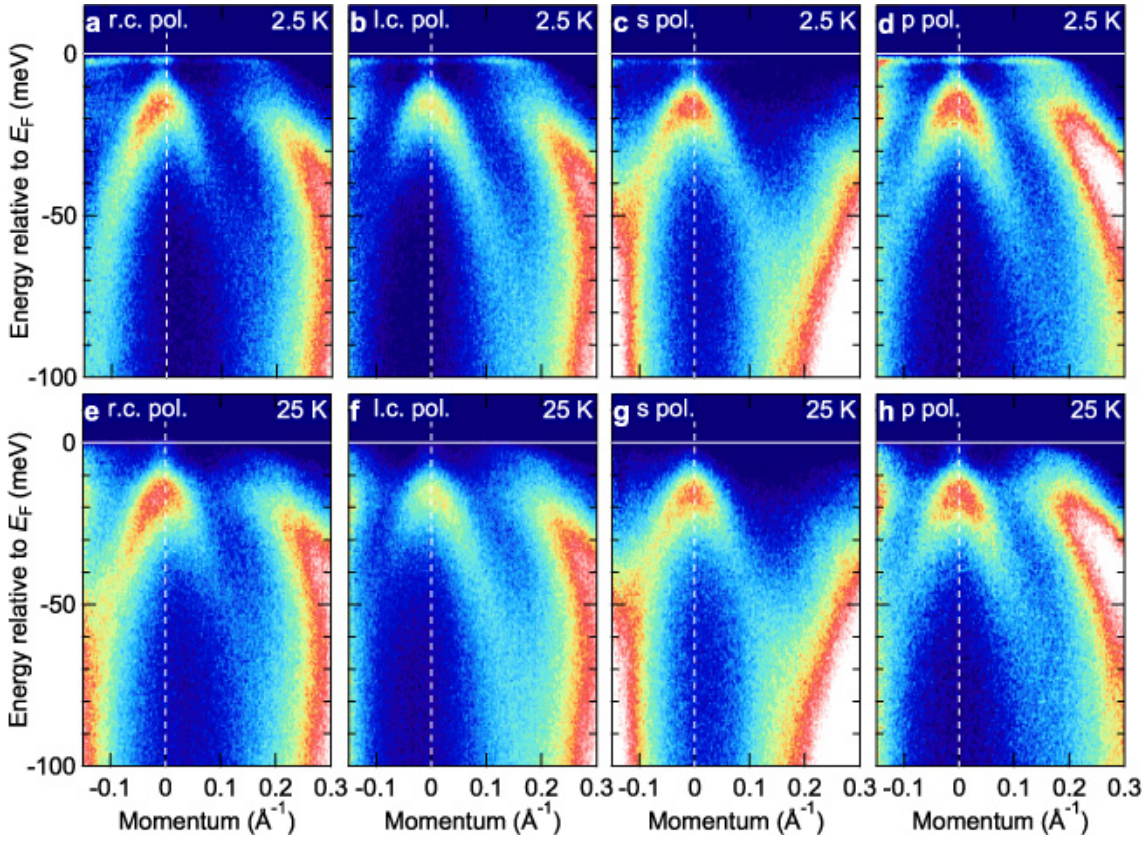

Fig. S8. Polarization-dependent intensity map below T_c (= 2.5 K) and above T_c (= 25 K). (**a-d**) Intensity map at 2.5 K measured with (a) right circular, (b) left circular, (c) *s*-, and (d) *p*-polarizations, respectively. (**e-h**) Intensity map at 25 K measured with (e) right circular, (f) left circular, (g) *s*-, and (h) *p*-polarizations, respectively.

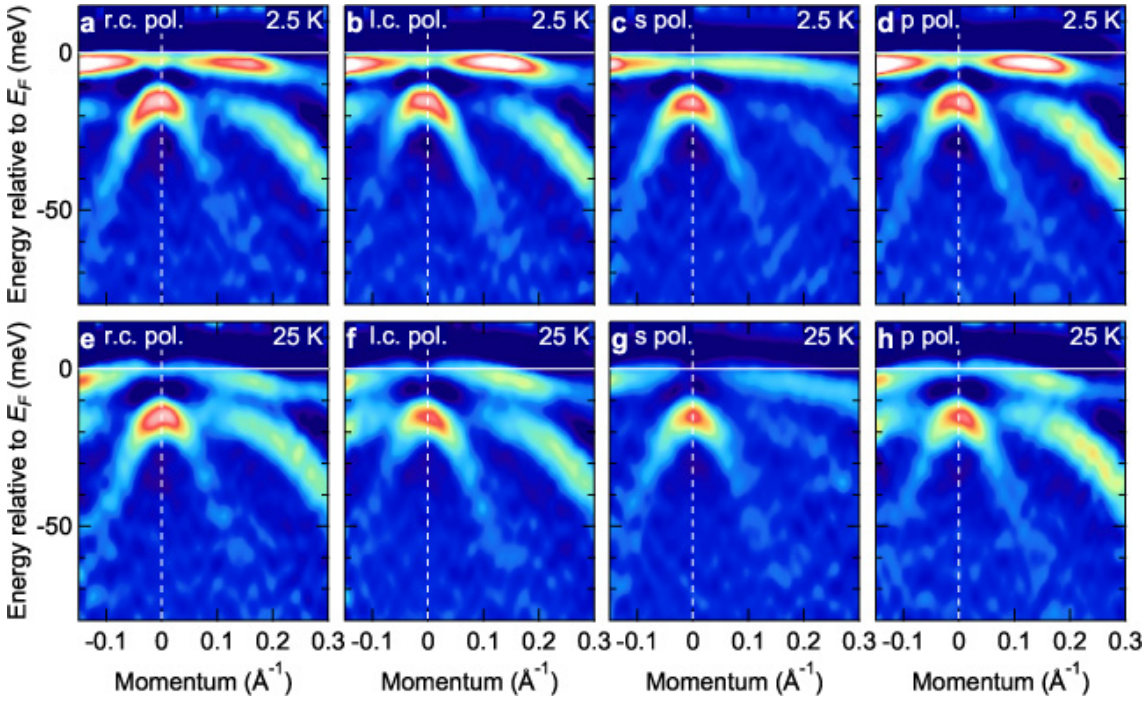

Fig. S9. Polarization-dependent second derivative map with respect to energy below T_c (= 2.5 K) and above T_c (= 25 K). (**a-d**) Intensity map at 2.5 K measured with (a) right circular, (b) left circular, (c) *s*-, and (d) *p*-polarizations, respectively. (**e-h**) Intensity map at 25 K measured with (e) right circular, (f) left circular, (g) *s*-, and (h) *p*-polarizations, respectively.

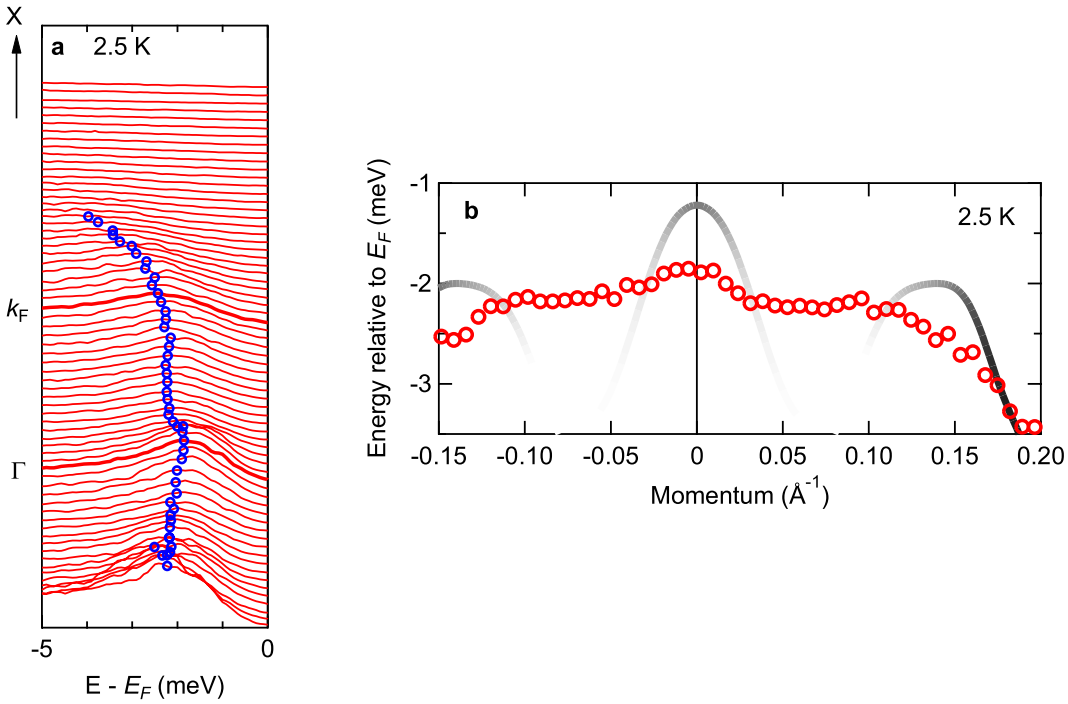

Fig. S10. The superconducting coherence peaks and BQP dispersions shown in Figs. 2(b) and 2(g) are plotted in an enlarged scale. These plots clearly show that the coherence peaks at $k \sim \Gamma$ is originated from the electron band just above E_F.

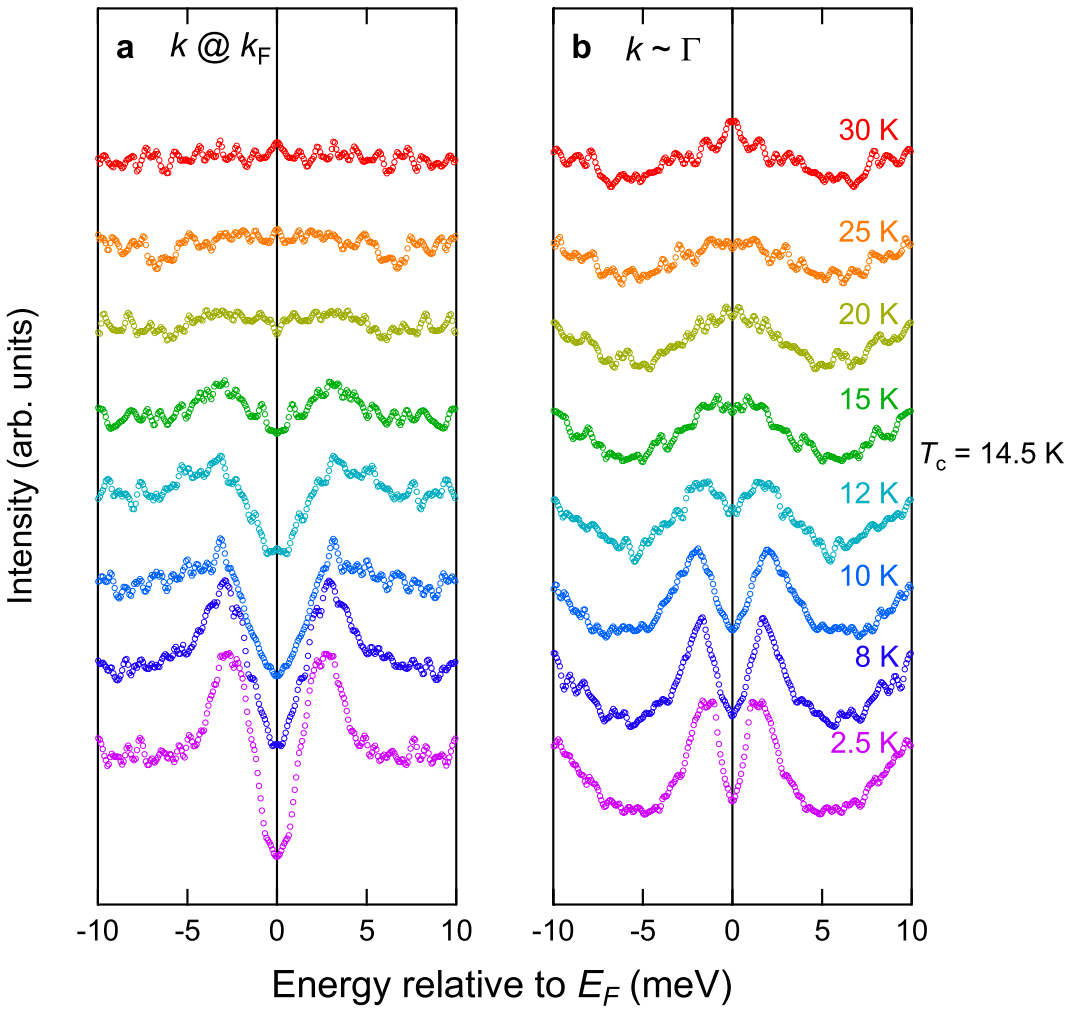

Fig. S11. Temperature dependence of symmetrized EDCs at $k = k_F$ and $k \sim \Gamma$. Temperature dependence of symmetrized EDCs at (**a**) $k = k_F$ of $x^2 - y^2$ hole-like band and (**b**) $k \sim \Gamma$ (bottom of the electron-like band), respectively.

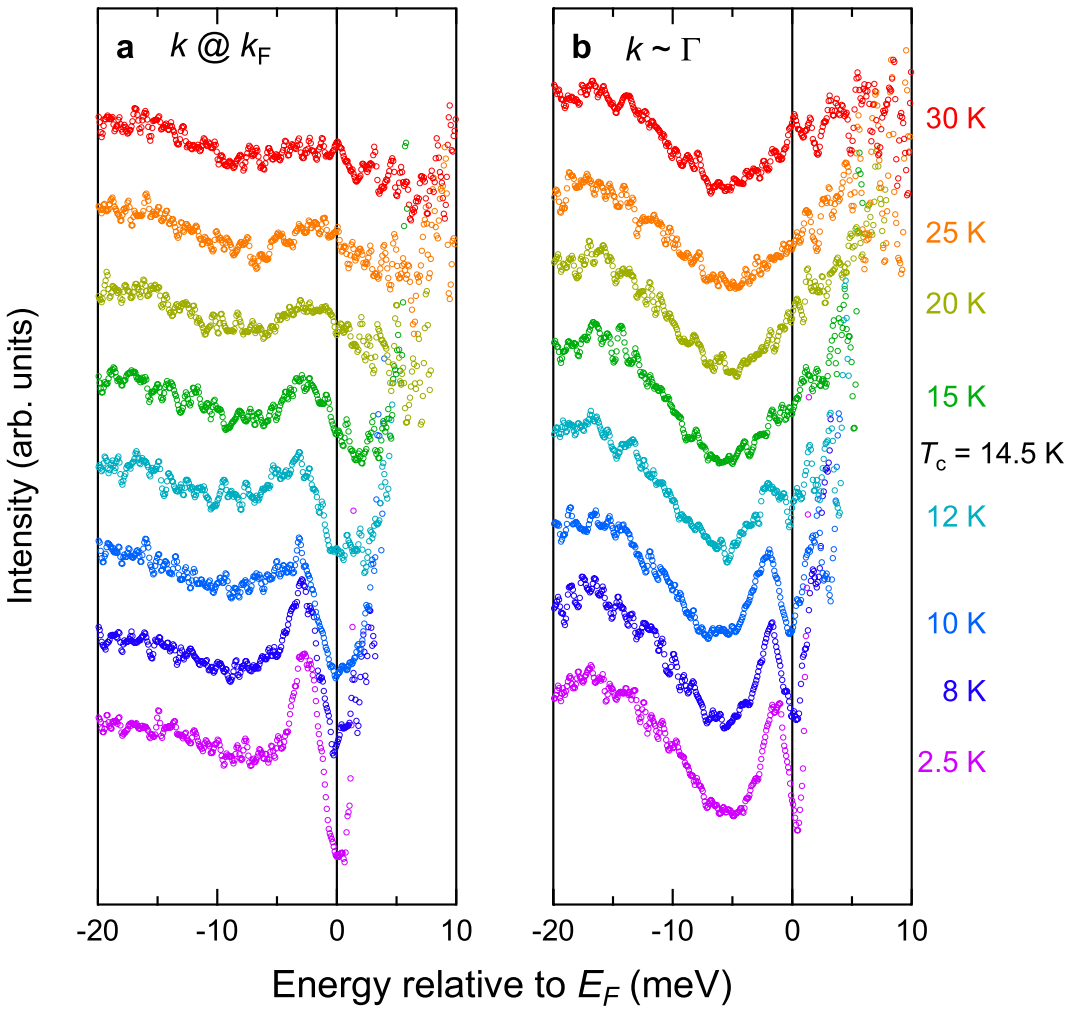

Fig. S12. Temperature dependence of FD-divided EDCs at $k = k_F$ and $k \sim \Gamma$. Temperature dependence of FD-divided EDCs at (**a**) $k = k_F$ of $x^2 - y^2$ hole-like band and (**b**) $k \sim \Gamma$ (bottom of the electron-like band), respectively.